



The 3D geometry of the Naxos detachment fault and the three-dimensional tectonic architecture of the Naxos metamorphic core complex, Aegean Sea, Greece

Henrik Linnros¹ · Reuben Hansman¹ · Uwe Ring¹ 

Received: 23 February 2018 / Accepted: 30 August 2018 / Published online: 26 September 2018
© The Author(s) 2018

Abstract

We reconstruct the three-dimensional (3D) geometry of the Naxos detachment fault and quantify E–W shortening associated with strong N–S extensional deformation. In addition, 3D reconstruction of the detachment indicates how it interacted with the underlying metamorphic sequence, as well as a set of concentric metamorphic isograds that formed during extensional deformation. For doing so, we used the software MOVE™ (Midland Valley Ltd.) to develop a 3D model of the Naxos metamorphic core complex (NCC) and the Naxos detachment fault. The model is constrained by structural data, metamorphic isograds, and fission-track ages from the footwall of the NCC. Our analysis shows that greater minimum amounts of E–W shortening correlate with higher metamorphic grade, ranging from 6 to 10% outside the migmatite dome and up to 17% within the migmatite dome. The metamorphic isograds around the migmatite dome are less intensely folded by E–W shortening than the lithologic layering. We conclude that this is because the isograd surfaces “froze-in” after folding had already started. Our model indicates that the isograds are cut by the brittle detachment, demonstrating that the final stages of top-to-the-NNE extension outlasted the formation of the metamorphic dome and the isograds. Despite some limitations of the 3D model, the outlined geometric reconstruction of a major extensional fault system in the central Aegean highlights: (1) the interplay between large-scale extension and temperature-dependant shortening perpendicular to the extension direction, (2) the evolution of metamorphism and migmatization, (3) the formation of metamorphic isograds, and (4) granitoid intrusions during extension and exhumation.

Keywords Three-dimensional tectonic model · Extension/shortening · Metamorphic isograds · Fission-track ages · Naxos metamorphic core complex · Aegean Sea · Greece

Introduction

The 3D architecture of metamorphic core complexes and relationships between the metamorphic evolution of their footwalls and the brittle detachments separating the footwalls from the brittlely deforming hanging walls have rarely been studied in detail. This is because the detachment faults are often eroded away above the updomed footwalls. Therefore, some critical details of the time-and-space evolution of the evolution metamorphic core complexes remain not well known.

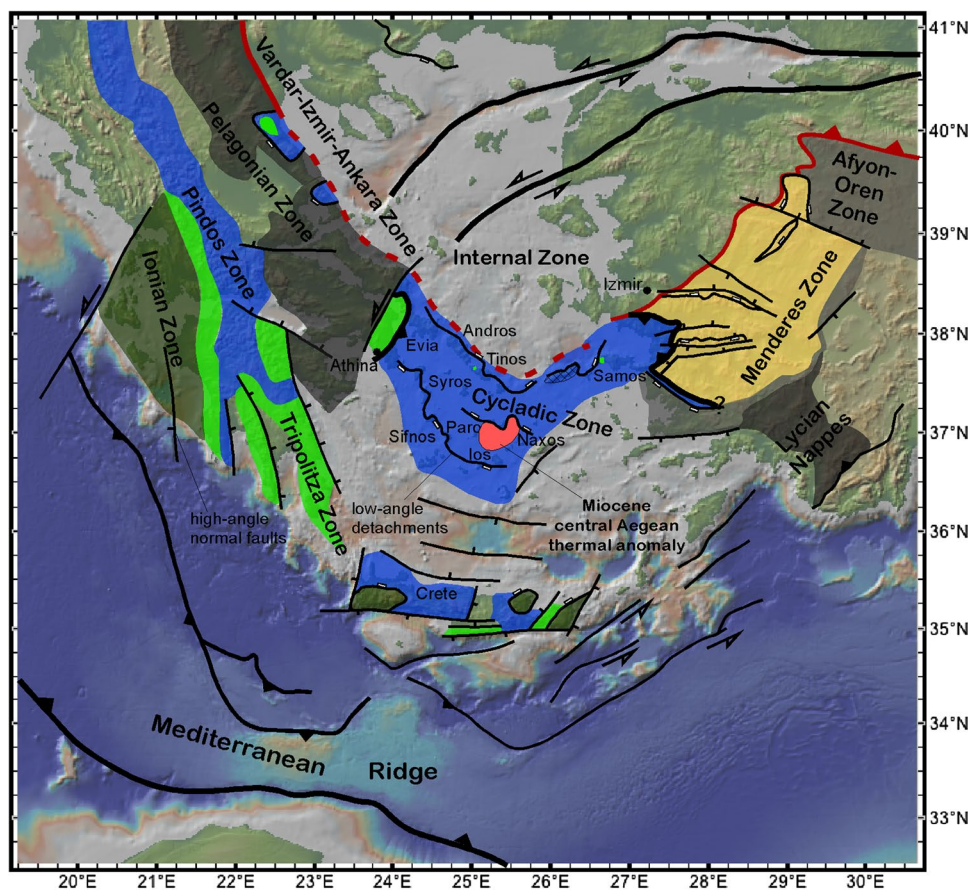
The Aegean Sea extensional province in the eastern Mediterranean (Fig. 1) is one of the best regions for studying metamorphic core complexes. A common problem with the Aegean metamorphic core complexes is that the detachment faults are either only exposed at the rims of islands or are not exposed at all. A good example illustrating that problem is reported in Brichau et al. (2007), whose thermochronological data showed that there must be three discrete detachment faults on Tinos Island instead of the single detachment fault as previously mapped. However, one of these detachment faults is not even exposed on Tinos. Therefore, the 3D geometry of the detachments remains largely elusive.

Recent advances in digital 3D modeling techniques and software packages now allow the construction of structures and rock layers for restoration to pre-deformed conditions to achieve a balanced interpretation. This ensures a geometrically, and therefore, geologically plausible model

✉ Uwe Ring
uwe.ring@geo.su.se

¹ Department of Geological Sciences, Stockholm University, 10692 Stockholm, Sweden

Fig. 1 Tectonic map of Aegean showing main tectonic zones and extensional fault systems; note small area of high-temperature metamorphism and exposed migmatites on Naxos and Paros islands in central Cyclades



(Chamberlin 1910; Hossack 1979; Maxelon and Mancktelow 2005; Zanchi et al. 2009a, b; Hansman and Ring 2018). These balanced 3D models have the potential to shed light on the interplay between structures and their temporal evolution. The 3D models can also help to constrain the geometry of structures that have been eroded allowing to discuss how these eroded structures interacted with still-observable structures.

Here we focus on the Naxos metamorphic core complex (NCC) (Fig. 2), which is arguably the most-studied core complex in the Aegean Sea extensional province. Pioneering mapping has established a concentric pattern of metamorphic isograds resulting from Miocene high-temperature metamorphism (Jansen and Schuiling 1976). Buick and Holland (1989) showed that Miocene metamorphism was a consequence of lithospheric scale extension and core-complex formation. Subsequently, Avigad et al. (2001) showed that the formation of the NCC by N–S extension was accompanied by folding due to E–W shortening. The surface geology indicates that this folding hardly affected the metamorphic isograds (Fig. 2) but it did affect the Naxos extensional detachment and the NCC below it. Furthermore, numerous zircon and apatite fission-track ages (ZFT and AFT) (Brichau et al. 2006; Seward et al. 2009) are available for the NCC and track

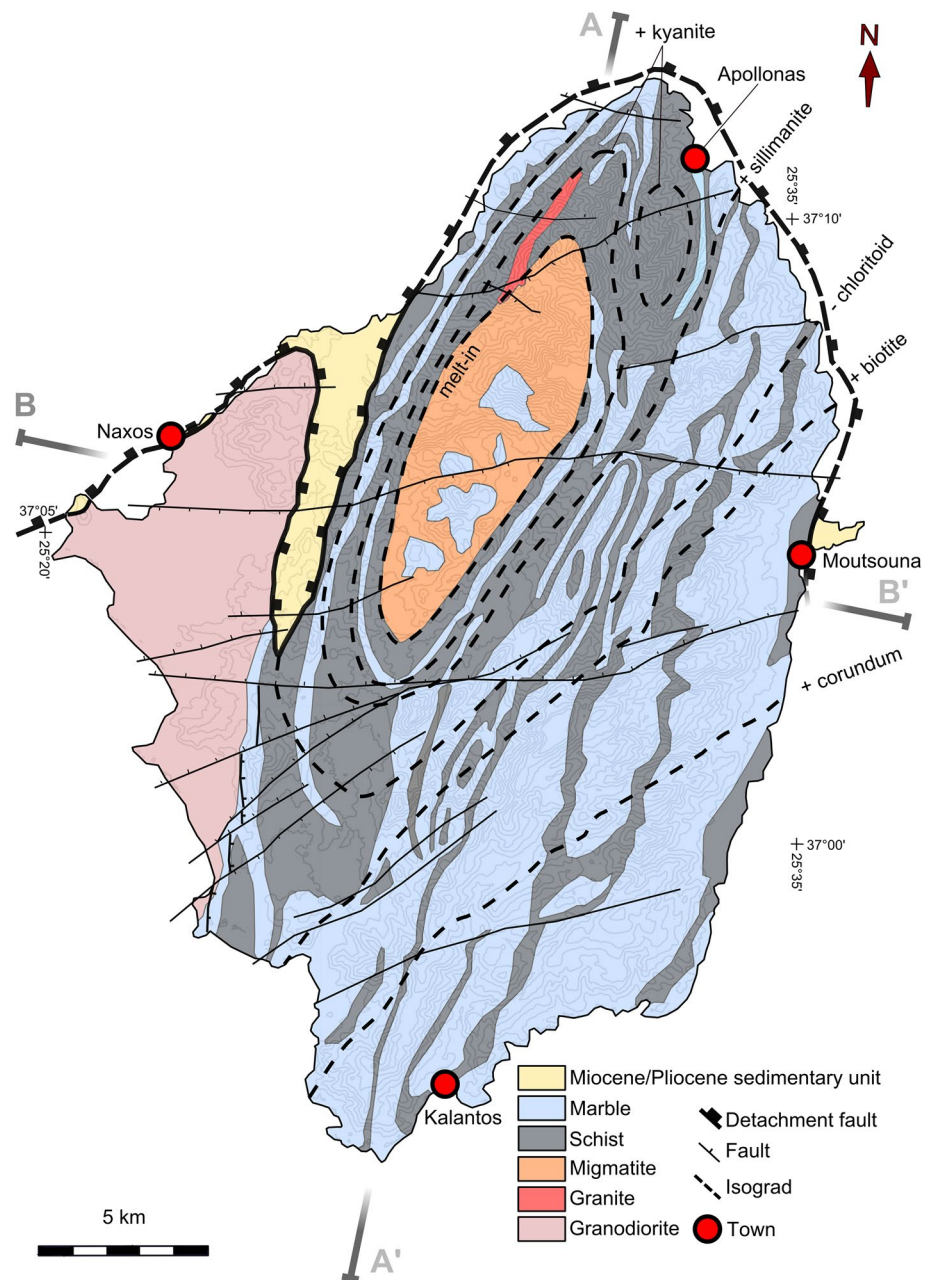
footwall cooling after the formation of the metamorphic isograds.

We present a 3D model of the NCC and the Naxos detachment fault using the Move™ software package. The main goal is to constrain the 3D geometry of the Naxos detachment fault, which is only exposed at the periphery of the island. Furthermore, we address: (1) the amount of E–W shortening associated with strong N–S extensional deformation; (2) how E–W shortening interacted with the detachment, the metamorphic sequence below the detachment and the metamorphic isograds; and (3) how contour maps of fission-track ages relate to extensional deformation. By visualizing the 3D geometry of the NCC, we show that E–W shortening increases with metamorphic grade. E–W folding commenced early during extension-related metamorphism and before the isograds formed. The folds, the isograds and the fission-track age contours are all cut by the brittle extensional detachment of the NCC.

Setting

The Hellenides in the eastern Mediterranean form an arcuate orogen to the north of the present-day active Hellenic margin (Fig. 1), which marks the site of NNE-ward subduction of

Fig. 2 Simplified geological map of Naxos modified from Kruckenberg et al. (2010) and Cao et al. (2013) with detachment fault, metamorphic isograds (Jansen and Schuil- ing 1976) and normal/oblique faults. Note chloritoid isograd cut by detachment in W; sillimanite, chloritoid and biotite isograds in NE cut by projected trace of detachment



the African plate beneath Eurasia. The Aegean Sea region in the Hellenides is a world-class example of large-scale continental extension above a retreating subduction zone. Most islands represent the updomed footwalls of metamorphic core complexes.

The Hellenides can be subdivided from top (north) to bottom (south) into (1) the Internal zone, (2) the Vardar–Izmir–Ankara suture zone, (3) the Pelagonian zone, (4) the Cycladic zone and (5) the External Hellenides (Dürr et al. 1978; Robertson et al. 1991) (Fig. 1). The Internal zone consists of continental fragments of the Eurasian plate, underneath which oceanic crust of Neotethys was subducted during Cretaceous convergence (Robertson et al. 1991). The

related suture is the ophiolitic Vardar–Izmir–Ankara zone. The underlying Pelagonian zone is a thrust belt (Franz and Okrusch 1992). The Cycladic zone consists of continental fragments of the Adriatic plate and can be subdivided into three tectonic units (Ring et al. 1999). These are, from top to bottom: (1) the non- to weakly metamorphosed Cycladic ophiolite nappe; (2) the high-pressure rocks of the Cycladic Blueschist Unit, the latter of which is lithologically subdivided from top to bottom into three separate members: (a) an ophiolitic mélangé, (b) a Permo-Carboniferous to latest Cretaceous passive-margin sequence and (c) a Carboniferous basement nappe. The Cycladic zone was intruded by S- and I-type plutons between ~17 and 11 Ma (Bolhar et al. 2010).

(3) The Basal unit as part of the External Hellenides (Triplitzta and Ionian zones in Fig. 1) consists of Mesozoic and early Cenozoic platform carbonates found in several tectonic windows (Avigad and Garfunkel 1989; Ring et al. 2001).

In the Cyclades of the central Aegean Sea, the Hellenide Orogeny commenced in the early Cenozoic causing subduction and sustained, downward-propagating high-pressure metamorphism between c. 53 Ma and c. 30 Ma (Wijbrans et al. 1990; Tomaschek et al. 2003; Ring et al. 2007). At c. 23 Ma, large-scale continental extension above the Hellenic subduction zone commenced (Thomson et al. 2009; Jolivet and Brun 2010; Ring et al. 2010). In general, extensional deformation progressed under greenschist-facies conditions, but in the central Cyclades (Naxos and Paros islands) a thermal anomaly expressed by the exposure of amphibolite-facies rocks and migmatites formed as a result of the extension (Fig. 2).

Geology of Naxos

The geology of Naxos consists of non-metamorphosed sedimentary and ophiolitic rocks above, and the Cycladic Blueschist Unit below the Naxos extensional detachment (e.g., Dürr et al. 1978; Buick and Holland 1989; Avigad et al. 2001). N–S extension on Naxos started at c. 20 Ma and continued until about 8 Ma (Keay et al. 2001; Brichau et al. 2006) and caused more than 80 km of extension (Ring et al. 2010, 2018). The footwall of the Naxos detachment consists of Permo-Carboniferous to latest Cretaceous passive-margin sequence and underlying migmatite, which formed in the Carboniferous basement (Fig. 2). The passive-margin sequence comprises mainly marble and schist showing evidence for an early blueschist-facies metamorphism in southern Naxos at pressure and temperature conditions of ~ 16 kbar and 580–610 °C at about 40 Ma (Avigad 1998; Peillod et al. 2017). The basement consists of migmatitic gneiss and marble.

Miocene lithospheric extension controlled crustal anatexis forming the migmatite dome in the central part of Naxos, minor leucogranite intrusions in the passive-margin sequence to the north, and the intrusion of a granodiorite body in the west of the island (Jansen and Schuiling 1976; Buick and Holland 1989). Jansen and Schuiling (1976) mapped six concentric metamorphic isograds indicating a strong thermal overprint, with increasing temperatures toward the migmatite dome (Fig. 2). The basement in the center of the migmatite dome reached conditions of partial melting at ~ 750 °C and 8.5 kbar. The metamorphic peak at the periphery of the migmatite dome ranges from 700 °C and 8.5 kbar to 500 °C and 5 kbar (Jansen and Schuiling 1976; Buick and Holland 1989). It has been suggested that melting occurred between ~ 20 Ma and 16 Ma as indicated

by U–Pb zircon ages from leucosomes and pegmatites (Keay et al. 2001). Based on Ar/Ar white mica and hornblende dating, Wijbrans and McDougall (1988) also argued that the peak of high-grade metamorphism occurred in the middle Miocene between about 20 and 16 Ma. U–Pb dating of zircon from metamorphosed amphibolites provided ages as young as 15–14 Ma, indicating that conditions conducive to zircon growth during high-temperatures have persisted even at younger ages (Martin et al. 2006; Bolhar et al. 2017). Ring et al. (2018) provided Rb–Sr multi-mineral ages of pegmatites and migmatites indicating that high-temperature metamorphic conditions and partial anatexis during top-to-the-NNE extensional shearing in the NCC lasted until about 14–12 Ma and that ductile shearing, fluid flow, and recrystallization persisted at least until about 10–9 Ma (Cao et al. 2017). Ring et al. (2018) showed that the isograds formed after the peak of high-temperature metamorphism and near-isothermal decompression at a stage when the rocks started to cool significantly.

U–Pb zircon dating provided ages of 15.4–11.3 Ma for the leucogranites (Keay et al. 2001). The granodiorite in west Naxos occupies a large-scale antiform and intruded at 13.2–12.3 Ma (Bolhar et al. 2010). Zircon (ZFT) and apatite (AFT) fission-track ages range from 25.2 to 9.3 Ma and 13.0 to 6.4 Ma, respectively (Brichau et al. 2006; Seward et al. 2009).

The basal sedimentary rocks above the Naxos detachment were largely deposited in a fluvial, partly marine environment (Rösler 1972; Kuhlemann et al. 2004). Foraminifera, nanoplankton, and gastropods indicate that the base is Aquitanian (23–20.5 Ma) and the top Burdigalian (20.5–16 Ma) in age (Angelier et al. 1978; Lisker 1993). Böger (1983) reported an early-to-middle Miocene age for limnic-fluvial successions at Moutsouna at the east coast. The deposition of fluvial sediments records the establishment of intermediate mountainous relief of increasing proximity south of the basin and a change of regular, rhythmic fluvial deposition to seasonal fanlomeratic deposition. The depositional environment is characterized by a coarsening upward trend, indicating increasing relief (Kuhlemann et al. 2004). Above the marine/fluvial sequences are terrestrial conglomerates, which are younger than 8 Ma (Sanchez-Gomez et al. 2002). The hiatus between about 16 and 8 Ma either means no deposition during that period or sediments have been eroded before 8 Ma.

Avigad et al. (2001) mapped large-wavelength, low-amplitude folds with axes subparallel to the extension direction. These folds formed during extensional deformation and folded the Naxos detachment surface. Ring et al. (2017) argued that large-wavelength folding due to E–W shortening was involved in controlling basin topography, implying that the folds formed during the onset of extension in the early Miocene. Ring et al. (2017) further argued that shortening

was an elastic response perpendicular to extension without the need for any externally imposed far-field shortening. This process seems to be restricted to regions with a highly ductile lower crust and a shallow brittle–ductile transition (Levy and Jaupart 2011) and provides an elegant solution explaining large-wavelength folding coeval with large-scale extension and the formation of migmatites (Rey et al. 2011).

Data

For constructing a 3D model of the Naxos detachment fault and the underlying metamorphic core complex, the geological maps of Naxos by Jansen and Schuiling (1976) and Cao et al. (2013) were combined with a digital elevation model from ASTER (USGS) rendering a ground surface with a spatial resolution of 30 m. Orientation data ($n = 560$) pertaining to bedding, foliation, and stretching lineations as well as layer contacts, metamorphic isograds, and interpreted cross sections (Jansen and Schuiling 1976; Jansen 1973, 1977a; Urai et al. 1990; Gautier et al. 1993; Lister and Forster 1996; Kruckenberg et al. 2010; Linnros 2016) were also used. The geology was simplified into four major units: (1) the Naxos extensional detachment, (2) the Miocene/Pliocene sediments

above the detachment, (3) the metamorphic sequence below the detachment, and (4) the granodiorite in west Naxos. The Naxos detachment fault was digitized after Gautier et al. (1993), Kruckenberg et al. (2010) and Cao et al. (2013) (Figs. 2, 3, 4). The detachment surface dips at angles ranging between 10° and 30° in the west and east of Naxos Island (Kruckenberg et al. 2010; Cao et al. 2013; Linnros 2016). In the east, the Miocene-to-Pliocene sedimentary rocks dip at 15° to the west above the Naxos detachment (Cao et al. 2013). In the west, the Miocene-to-Pliocene sedimentary rocks are exposed in a N–S trending syncline. The thickness of these rocks is considered to be ~ 200 m on account of their reported thickness on nearby Paros Island (Sanchez-Gomez et al. 2002).

The migmatite at the bottom of the metamorphic sequence is modeled as two subdomes based on the detailed mapping by Kruckenberg et al. (2010). The schist and marble succession mantles the migmatite dome. The marble contains Triassic fossils and is stratigraphically younger and structurally above the schist (Jansen 1973, 1977a; Dürr et al. 1978). Schist and marble are intensely isoclinally folded and imbricated with each other (Dürr et al. 1978; Urai et al. 1990).

The metamorphic isograds formed during ongoing extension and after the peak of amphibolite-facies metamorphism.

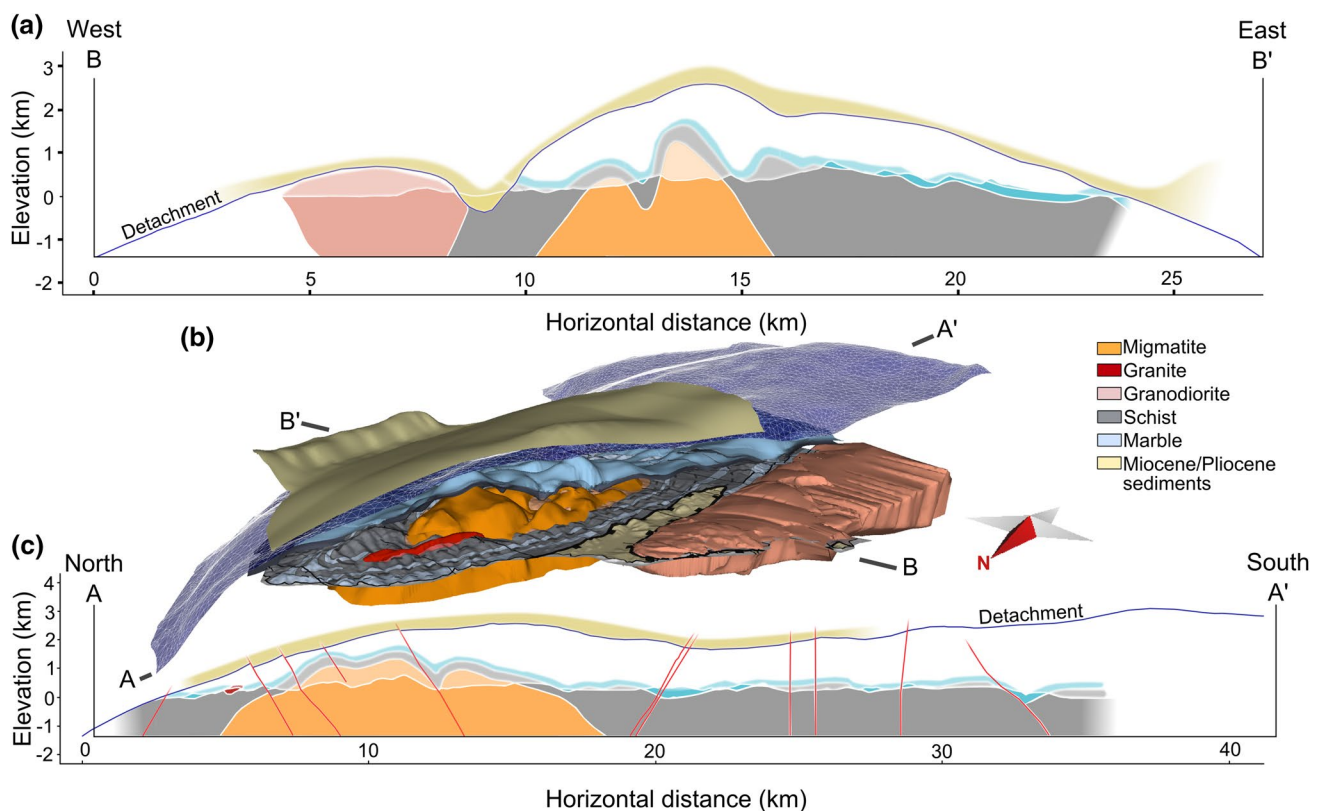


Fig. 3 E–W and N–S profiles of modeled rock units and detachment surface; also showing view of 3D model viewed from NW. Note intensity of folding increases toward migmatite dome in E–W cross section; normal faults cut detachment in N–S cross section

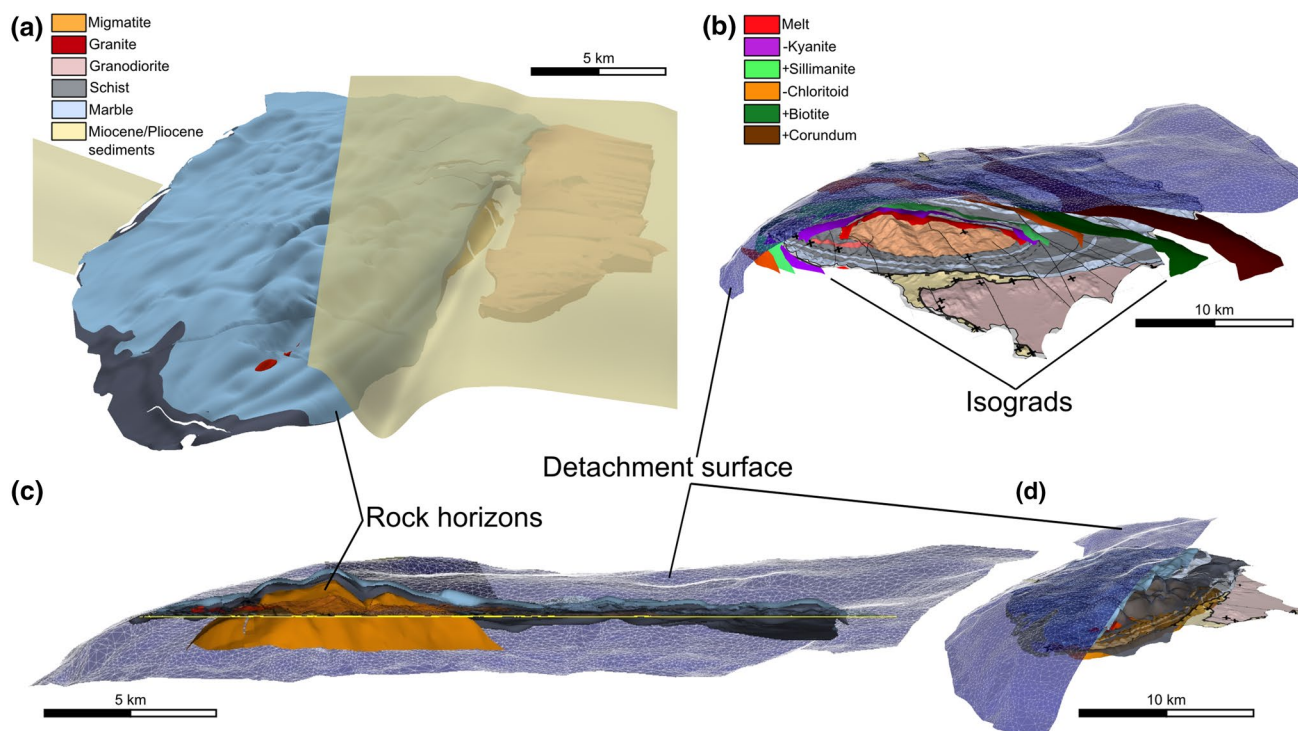


Fig. 4 **a** Modeled rock units seen from NNW. **b** Detachment surface 3D layer seen from W in 12° profile. **c** View from NNW of detachment surface clipped at 12° profile line; rock units extend to

–1500 m while detachment extends to maximum of –3500 m; spatial dimensions of model about 45 × 35 × 9 km

The mapping of the isograds by Jansen and Schuling (1976) (Fig. 2) shows that the chloritoid isograd is cut by the Naxos detachment in the west of the island. In the northeast, the kyanite, chloritoid, and biotite isograds are cut by the projected detachment (Lister and Forster 1996, their Fig. 9.3).

There are a number of E–W striking normal and NE-striking oblique normal faults (Fig. 2), which were modeled and used in section balancing as described in Linnros (2016). However, displacement on these faults is limited and they had no significant effect on the geometry of the detachment.

Method

For our reconstruction we used the structural modeling software MOVE™ (Midland Valley Ltd 2015.1). MOVE™ is a software suite that allows the construction of structural geological models in 2D and 3D. MOVE™ can kinematically restore a 2D or 3D model to an undeformed state to test for geometrical consistency, such as maintained rock volume between deformed and undeformed states. All data were imported into MOVE™ and 14 2D cross sections were created. Normal faults in these sections were restored using the move-on-fault 2D modules simple shear algorithm. This algorithm maintains the area between layers, based on the

details in Verrall (1981), Gibbs (1983) and Withjack and Peterson (1993). The line-length unfolding algorithm was used for restoring folds in 2D sections. The deformed layers are restored into straight lines by rotating the limbs of the folds and maintaining the layers' lengths. The interpreted cross sections used from previous workers were modified over a series of restorations to achieve geometrically consistent 2D sections. The detachment is constrained by its surface outcrop. It cannot be balanced, as there is nothing to compare its line length to. However, it geometrically matches the surface data and this is all that can be done. The balanced cross sections were interpolated to create the 3D surface of the Naxos detachment, the Miocene/Pliocene sediments above the detachment, the metamorphic sequence and the granodiorite in western Naxos below the detachment.

The 3D structural model was then sliced in E–W and N–S 2D sections, which are perpendicular and parallel to the migmatite dome axis, respectively. The sections were used to restore the faulting and folding deformation in the model as discussed above to estimate E–W shortening of the NCC.

Applying standard kinematic restoration methods to the mid-crustal rocks below the detachment has limitations. Because the schist–marble sequence is isoclinally folded and imbricated and this deformation occurred before large-scale extension and the associated formation of the Naxos detachment, we largely ignored the complex folding and assumed

a layer-cake model with the marble above the schist. Our model restores the marble–schist sequence by constant line length, which assumes plane strain and no volume change. These assumptions are not accurate for mid-crustal rocks as: (1) metamorphism may have caused rock volume to change. (2) Ductile deformation may have produced thickness variations of the layers. Both processes would affect line length balancing. (3) Furthermore, extensional deformation was a combination of pronounced N–S extension and minor E–W shortening causing the rock volume to move perpendicular to the 2D sections. Given these limitations, the model is useful in providing a minimum amount of shortening.

The migmatite and the granodiorite were not balanced. In our modeled sections the migmatite is filling the space below the schist–marble sequence to a depth of -1.5 km. Therefore, the geometry of the migmatite in our cross sections is basically a result of the infolded schist–marble sequence and this geometry directly matches the double-dome geometry mapped by Kruckenberg et al. (2010). The granodiorite also fills the space below the Naxos detachment to a depth of -1.5 km.

The apatite and zircon fission-track ages from Brichau et al. (2006) and Seward et al. (2009) were used to generate fission-track age contour maps using an ordinary kriging method in MOVE™. For the contouring only the central ages without any errors could be used, but the 2σ uncertainties are shown for each data point in the contour maps.

Results

Geometry of rock sequence and Naxos detachment

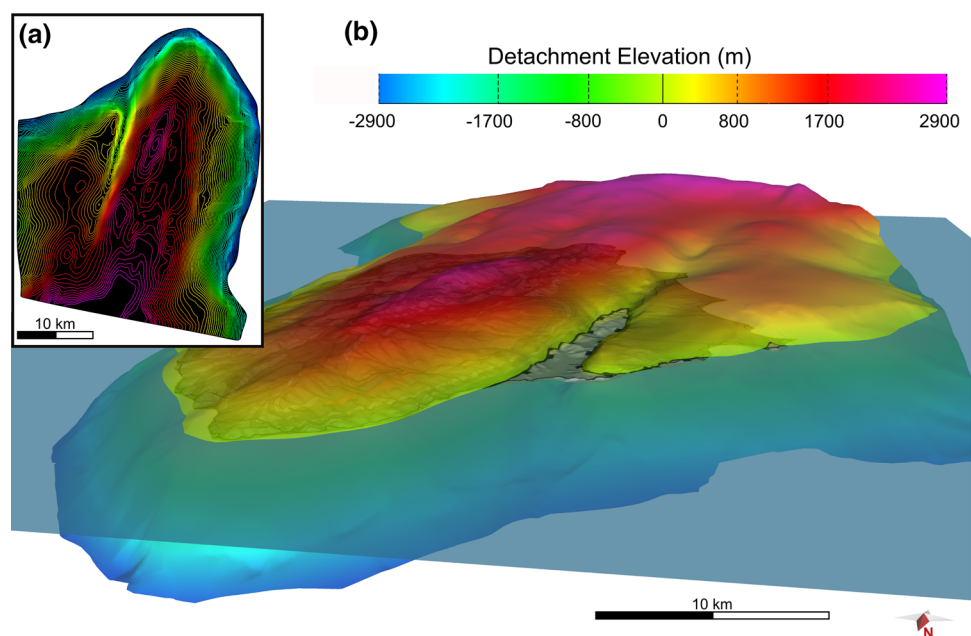
The results of the 2D and 3D reconstructions are shown in Fig. 3 through Fig. 8. Figure 3 shows geometrically viable N–S and E–W cross sections of the metamorphic sequence and the detachment surface. In the E–W cross section, the modeled detachment surface is distinctly less folded than the underlying metamorphic sequence. This visualized finding directly results from the map relations (Fig. 2) showing the schist–marble succession distinctly more intensely folded than the detachment surface. The folding of the schist–marble sequence has wavelengths decreasing and amplitudes increasing close to and in the migmatite dome, the latter of which occurs in a major, broad antiform of the detachment surface. The detachment surface cuts the E–W folds west of the migmatite dome (Fig. 3).

The detachment drapes across the entire island. Its dip is generally flat above the island ($< 15^\circ$ to the north) and then the dip angle increases to 30° – 45° in the north and east (Figs. 3, 4, 5). Folding with N–S axes in the Miocene–Pliocene sediments above the detachment also mimic that of the detachment. In the N–S cross section, the normal faults cut the detachment (Fig. 3c).

Metamorphic isograds

The modeled metamorphic isograds and the detachment surface are shown in Fig. 6. The 3D shape of the isograds has been extended above the earth's surface to visualize

Fig. 5 Modeled detachment surface viewed from NW; flat transparent surface represents sea level. Inset shows 2D contour map of detachment surface. Elevation shown by color coding, same scale for 2D and 3D maps



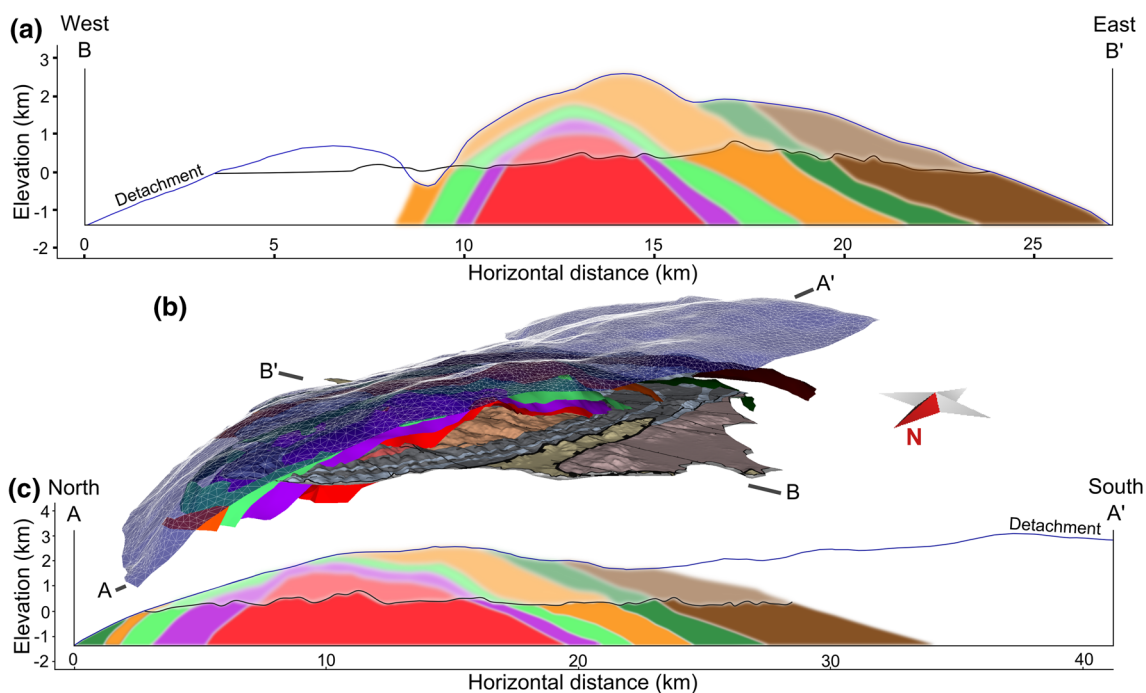


Fig. 6 E–W (a) and N–S (c) profiles of metamorphic isograds below detachment surface. **b** 3D model viewed from NW, isograds and detachment surface draped over geological map; for legend of isograds see Fig. 4

their relation with the projected Naxos detachment surface (Fig. 2). Both cross sections show that the isograds are cut by the detachment. This is in line with the field observations by Jansen and Schuiling (1976) as shown on the map (Fig. 2), where the chloritoid isograd is cut by the detachment in the synform in western Naxos. The isograds’ surfaces are distinctly less folded than the metamorphic sequence.

E–W shortening

The average amount of E–W shortening is estimated at 11% (Table 1). However, E–W shortening shows striking differences in the N–S direction (Fig. 7). The greatest amount of shortening of 17% occurs in the central part of the migmatite dome and then decreases to the north and south to less than 10% (Fig. 7). Furthermore, the amplitudes of the folds increase and the wavelengths decrease in the migmatite dome (Fig. 3a), which is well expressed in the migmatite itself being more intensely folded than the

Table 1 Calculations of shortening for various E–W profiles (refer to Fig. 7 for profile locations)

| Model-/section nr. | Marble (m) | Schist (m) | L_f (m) | Average L_0 (m) | Extension/shortening (%) |
|--------------------|------------|------------|-----------|-------------------|--------------------------|
| Section 1 | 16,162 | 16,047 | 16,104.5 | 14,784 | –8 |
| Section 2 | 16,553 | 16,493 | 16,523 | 15,100 | –9 |
| Section 3 | 16,762 | 16,548 | 16,655 | 14,959 | –10 |
| Section 4 | 16,007 | 15,949 | 15,978 | 14,567 | –9 |
| Section 5 | 17,252 | 17,189 | 17,220.5 | 14,270 | –17 |
| Section 6 | 15,788 | 15,753 | 15,770.5 | 13,719 | –13 |
| Section 7 | 15,628 | 15,612 | 15,620 | 13,646 | –13 |
| Section 8 | 13,333 | 13,252 | 13,292.5 | 11,827 | –11 |
| Section 9 | 7957 | 7925 | 7941 | 7508 | –6 |
| Average shortening | | | | | –11 |

L_f deformed length, L_0 unfolded line length

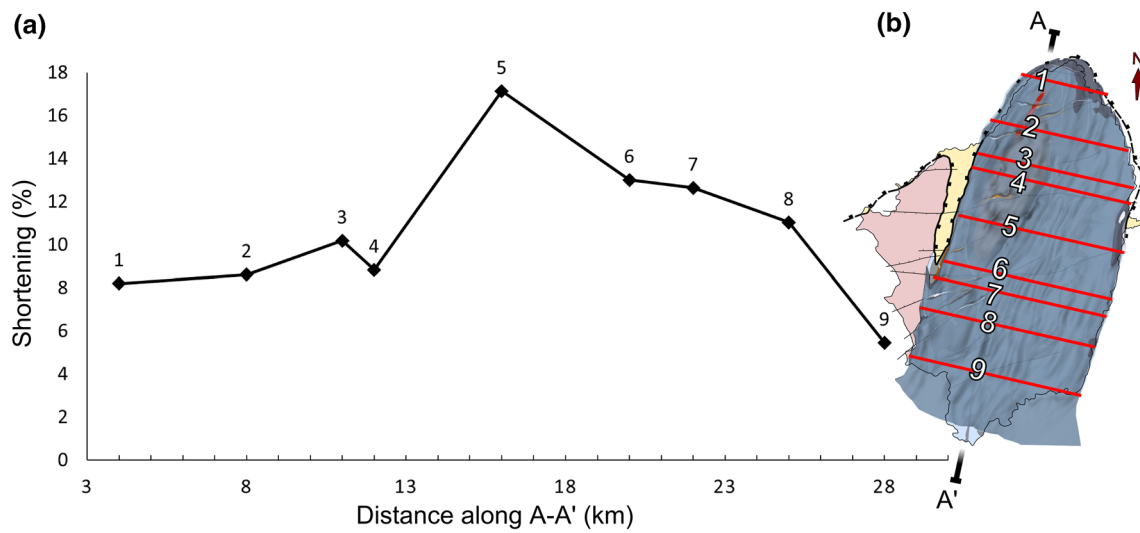


Fig. 7 Estimates for minimum shortening of nine E–W profiles across Naxos; refer to Table 1 for data. Note increased shortening towards migmatite dome where syn-extension metamorphic temperatures are highest

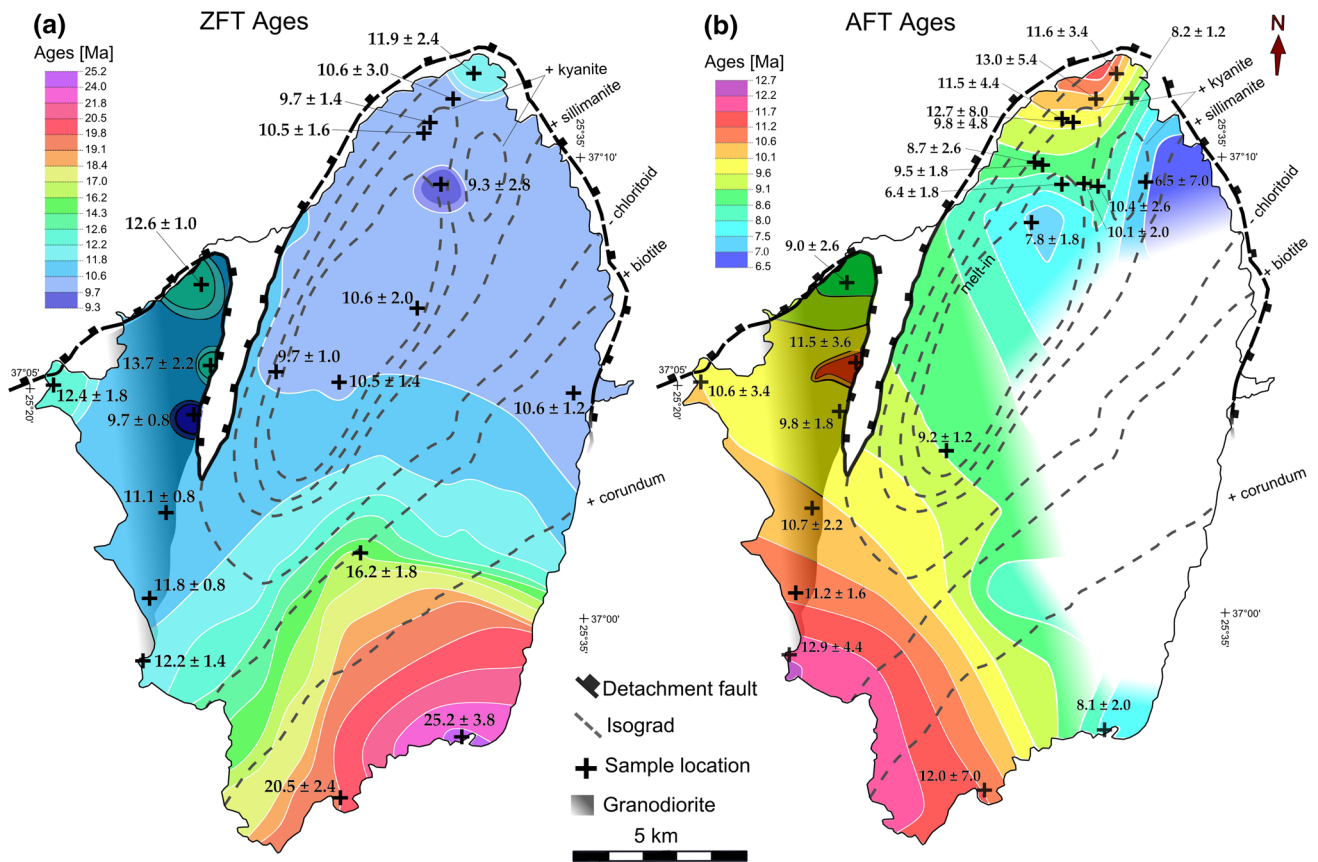


Fig. 8 Contour maps for zircon (left) and apatite (right) fission-track ages (Seward et al. 2009; Brichau et al. 2006); S-to-N younging trend of ages despite apparent artifacts in contouring due to differential data coverage

detachment surface. The shortening results represent a minimum amount, as the geology was simplified for the model, which means that folding in Naxos may actually be more intense than this study implies.

Fission-track age contour map

The contouring of the fission-track ages (Fig. 8) depicts a general younging trend toward the N in the direction of hanging-wall transport at the Naxos detachment. This trend is especially obvious for the ZFT ages. ZFT show old ages of 25.2 ± 3.8 Ma and 20.5 ± 2.4 Ma in southern Naxos indicating that these rocks were hardly affected by the Miocene high-temperature metamorphism and the formation of the Naxos migmatite dome and are in line with Rb–Sr multi-mineral ages reported by Peillod et al. (2017). The relatively old ZFT age of 11.9 ± 2.4 Ma in the N does not fit this general trend. The pattern of AFT ages is more complicated, especially the relatively old ages in the far north of Naxos.

Seward et al. (2009, their Fig. 3) plotted their fission-track ages along a N–S section parallel to the direction of extensional shearing. Their profile shows that the fission-track ages slightly increase in the north close to the trace of the projected Naxos detachment. Seward et al. (2009) explained this curved geographical distribution by the juxtaposition of the exhuming footwall against the colder hanging-wall resulting in the downward deflection of the isotherms towards the hanging wall. Therefore, the rocks close to the detachment would cool through a given (shallow-level) isotherm earlier than rocks further south close to the migmatite dome.

Discussion

Main findings

Before discussion of our main findings, it seems warranted to stress some of the limitations of our 3D model here again. The main goal was to project the Naxos extensional detachment across the entire island for analysing tectonic interactions of the detachment with the underlying metamorphic core complex. The reconstruction of the detachment is constrained by its surface outcrops on the eastern and western side and its projected trace around the northern tip of the island. More critical are the assumptions we had to make for reconstructing the metamorphic sequence below the detachment by simplifying the ductile deformation of the schist–marble sequence and not including the migmatite and granodiorite in the balancing exercise. Because of these limitations, the model is only useful in providing minimum amounts of E–W shortening. The amount of extension on the Naxos detachment cannot

by quantified with our approach at all, but is fairly well constrained to > 80 km (Ring et al. 2018).

The geometric analysis and visualization of the Naxos geology have shown that there is a correlation between the minimum amount of E–W shortening and exposed metamorphic grade with more shortening related to higher metamorphic grade. This trend is also expressed by the tightness of the folds (Fig. 3). Another main finding is that folding due to E–W shortening affected the metamorphic layering distinctly more than the metamorphic isograds that formed in this layering, and also more than the detachment surface. The latter is, for instance, highlighted in the E–W cross section in Fig. 3, where the long-wavelength folding of the detachment cuts the short-wavelength folding in the metamorphic section. Because we only have minimum amounts of shortening it is implied that the difference in the intensity of folding of the metamorphic sequence and the detachment surface is more drastic. This suggests that the folding commenced early and deep during extension as it affected the deep-seated metamorphic sequence more than subsequent isograd formation and the brittle detachment surface. An early onset of folding more or less concurrent with the onset of large-scale extension is supported by Virgo et al. (2018), who studied folding of amphibolite layers within marble in the Naxos migmatite dome. These authors also concluded that folding occurred during viscoelastic flow between 20 and 16 Ma.

The relation of E–W shortening and metamorphic grade indicates that folding is intimately related to high-temperature metamorphism. The main foliation formed or was pervasively reworked during high-temperature metamorphism and was deformed by the E–W folds. However, the metamorphic isograds crosscut the main lithology-parallel foliation (Fig. 2), consistent with the findings of Jansen and Schuiling (1976) and Ring et al. (2017). The folding of the isograds occurred during cooling after near-isothermal decompression (Jansen 1977b) when the metamorphic rocks were already considerably exhumed from about 35 to 15–18 km (Ring et al. 2018). Ring et al. (2018) showed that the isograds formed at 14–12 Ma and that isograd formation was a diachronous event proceeding from south to north. Such a relatively late formation of the isograds is in line with our visualized finding that the isograds are distinctly less folded than the main foliation and the lithologic layering. Overall, our result that the amount of E–W shortening becomes less during exhumation is in line with numerical modeling by Rey et al. (2011), who showed that horizontal shortening is intense in the deep crust and horizontal extension dominates higher up in the crust. However, it needs to be emphasized that the upper-crustal detachment is also folded and that there was also pronounced N–S extension in the amphibolite-facies rocks at the bottom of the metamorphic section.

The isograds' surfaces are distinctly stretched in N–S indicating ongoing ductile N–S extension during and after their formation. This agrees with ages of ~12–9 Ma for late retrograde deformation in the north of Naxos (Cao et al. 2017; Ring et al. 2018). The contouring of the FT ages displays a robust younging to the north tracking footwall cooling in the brittle crust. The detachment surface progressively cuts down to the north. The ZFT ages provide a minimum age for isograd formation. The strong south-to-north asymmetry of the ages also suggests that the isograds started to form in the south and then their formation propagated northward.

Tectonic interpretation

Large-scale lithospheric extension in Naxos was underway by 20 Ma (Wijbrans and McDougall 1988; Keay et al. 2001; Ring et al. 2018) and subsequently controlled high-grade metamorphism and partial melting, the intrusion of leucogranites and pegmatites, E–W folding, and the intrusion of the Naxos granodiorite. The first effects of extension are the formation of the E–W folds as well as high-temperature metamorphism and partial melting; followed by the various granitic/pegmatitic intrusions (Buick and Holland 1989; Lister and Forster 1996; Avigad et al. 2001; Brichau et al. 2006; Seward et al. 2009; Bolhar et al. 2010, 2012; Cao et al. 2013; Ring et al. 2018) (Fig. 9a). Lower crustal flow advected heat causing high-temperature metamorphism and partial melting during exhumation after 20 Ma. There was probably a lag time between the onset of extension triggering lower crustal flow and partial melting. Ring et al. (2018) argued that an age of 18.4 ± 0.2 Ma (Keay et al. 2001) reflects the first crystallization of migmatite. The migmatites and partial melts were attracted by a developing antiform and, therefore, now occur within a large-wavelength antiform of the detachment surface. The detachment surface at this stage was situated much further south and was, together with the depositing sediments less affected by E–W shortening.

According to the experiments by Lévy and Jaupart (2011), large-scale extension immediately triggered E–W shortening and folding, which is in line with our findings. Ring et al. (2017) argued that the folds are an elastic response perpendicular to extension without the need for externally imposed far-field shortening [see also Gessner et al. (2013) for similar early Miocene folding in the adjacent Menderes Massif of western Turkey]. This process seems to be restricted to regions with a highly ductile lower crust and a shallow brittle–ductile transition (Lévy and Jaupart 2011). A striking similarity between large-wavelength folding in Naxos and the northern Menderes Massif is the intrusion of huge granodiorite bodies into folding-related antiforms associated with large-scale extension.

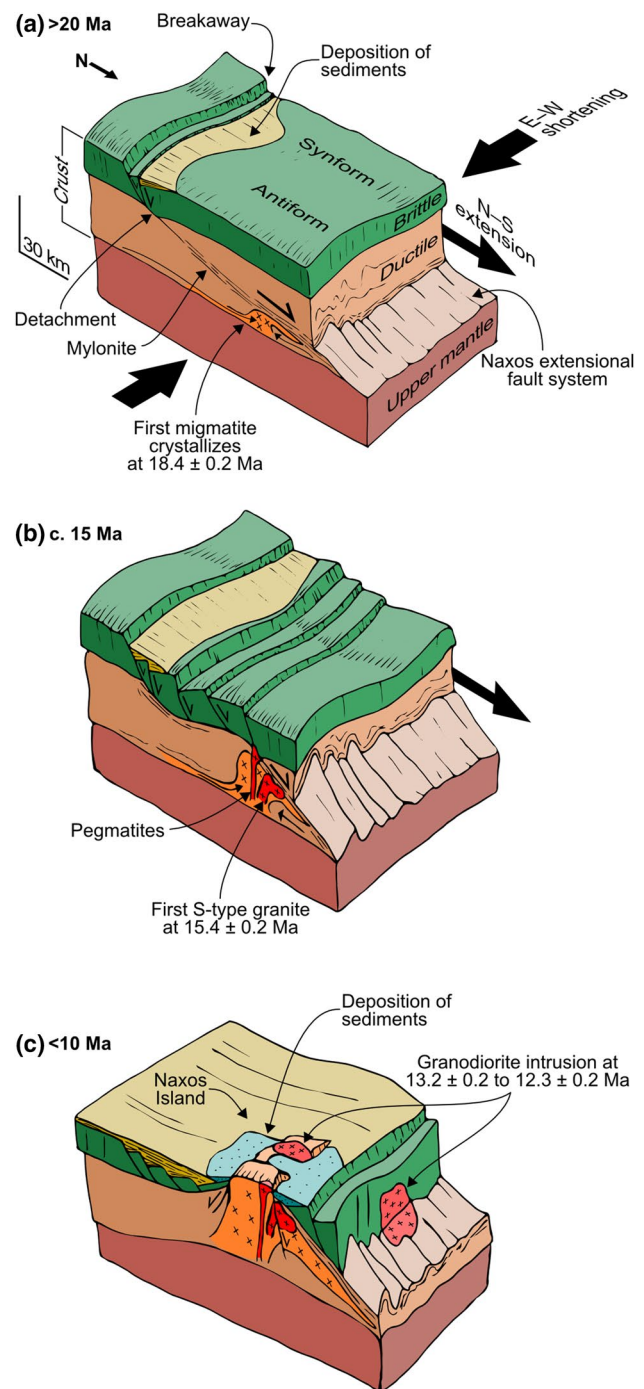


Fig. 9 Proposed tectonic interpretation for Naxos extensional fault system and evolution of high-temperature metamorphism and intrusions in footwall. **a** Inception of extensional deformation in early Miocene, deposition of sediments and high-temperature metamorphism and migmatization in lower crust; N–S extension coeval with E–W shortening. Note that breakaway and migmatization are >80 km apart from each other. **b** Intermediate stage of extensional deformation, continued migmatization, intrusion of pegmatites and S-type granites; footwall of Naxos extensional fault system moves to south toward breakaway. **c** Advanced stage of extensional deformation after intrusion of large I-type granodiorite and renewed sedimentation at c. 8 Ma in hanging wall of high-angle normal faults

During the second conceptual step (Fig. 9b), the evolving core complex has been exhumed toward the south, migmatites kept forming and pegmatites and S-type granites intruded. At this stage, the southern end of the Naxos migmatite dome started to cool significantly as indicated by a zircon fission-track age of 16.2 ± 1.8 Ma (Seward et al. 2009) (Fig. 8). Brichau et al. (2006) and Ring et al. (2018) showed that the Naxos extensional fault system was rapidly moving and therefore exhumation of the footwall is responsible for near-isothermal decompression of the metamorphic rocks. At the end of this decompression the isograds formed. Since the footwall was exhumed toward the south, the isograds started to ‘freeze in’ in the south and then isograd formation propagated to the north. Northward-propagating isograd formation during ongoing N–S extension explains the stretched outline of the isograds (Fig. 2). Isograd formation occurred when the thermal gradient was highest, i.e., at the turnover from near-isothermal decompression to pronounced cooling at crustal levels of 15–18 km (Ring et al. 2018). At the end of step 2, the Naxos I-Type granodiorite intruded into the other (western) major antiform of the detachment surface.

During the final step of our interpretation (Fig. 9c), the brittle Naxos detachment was finally juxtaposed with the NCC between 10 and 8 Ma. At that time all isograds had formed and the cooling through the zircon and apatite fission-track closure temperatures (240 ± 20 and 110 ± 10 °C, respectively; Reiners and Brandon 2006) has been completed. High-angle normal faulting started during and after final juxtaposition as the normal faults cut the detachment surface. It seems conceivable that during final juxtaposition the wider Naxos area became emergent and hanging-wall rocks were eroded causing the hiatus in depositional ages. Deposition of the post 8 Ma terrestrial sediments was then controlled by high-angle normal faulting.

Concluding remarks

Our 3D analysis of the Naxos geology shows that the amount of E–W shortening strongly correlates with exposed metamorphic grade and is most intense in the deep-seated migmatite. Both the Naxos detachment surface and the metamorphic isograds straddling the migmatite dome show less intense folding. This shows that folding due to E–W shortening commenced early during large-scale extension and affected the deep-seated rocks most. The metamorphic isograds formed later and at shallower crustal levels and were therefore less folded. The contouring of the FT ages displays a robust younging to the north tracking footwall cooling and isograd formation. Later, the isograds are cut by the brittle detachment, demonstrating that the final stages of top-to-NNE extension outlasted the formation of the metamorphic dome and isograds. Despite the limitations of our 3D

model, the outlined geometric reconstruction of the large-scale Naxos extensional fault system in the central Aegean highlights the complex interplay between large-scale extension and temperature-dependant shortening perpendicular to the extension direction. The 3D model allows to discuss the evolution of metamorphism and migmatization, the formation of metamorphic isograds, and granitoid intrusion during extension and exhumation.

Acknowledgements We acknowledge the use of the Move Software Suite granted by Midland Valley Ltd Academic Software Initiative. Funded by Vetenskapsrådet (Swedish Research Council, VR 621-2012-4549). We thank an anonymous reviewer and Ingo Braun for critical comments and the editor for handling our manuscript.

Open Access This article is distributed under the terms of the Creative Commons Attribution 4.0 International License (<http://creativecommons.org/licenses/by/4.0/>), which permits unrestricted use, distribution, and reproduction in any medium, provided you give appropriate credit to the original author(s) and the source, provide a link to the Creative Commons license, and indicate if changes were made.

References

- Angelier J, Glauçon G, Müller C (1978) Sur l’existence et la position tectonique du Miocène inférieur marin de l’archipel de Naxos (Cyclades, Grèce). *Comptes Rendus Acad Sci Paris* 286:21–24
- Avigad D (1998) High-pressure metamorphism and cooling on SE Naxos (Cyclades, Greece). *Eur J Mineral* 10(6):1309–1319
- Avigad D, Garfunkel Z (1989) Low-angle faults above and below a blueschist belt—Tinos Island, Cyclades, Greece. *Terra Nova* 1(2):182–187
- Avigad D, Ziv A, Garfunkel Z (2001) Ductile and brittle shortening, extension-parallel folds and maintenance of crustal thickness in the central Aegean (Cyclades, Greece). *Tectonics* 20(2):277–287
- Böger H (1983) Stratigraphische und tektonische Verknüpfungen kontinentaler Sedimente des Neogens im Ägäis-Raum. *Geol Rundsch* 72(3):771–813
- Bolhar R, Ring U, Allen CM (2010) An integrated zircon geochronological and geochemical investigation into the Miocene plutonic evolution of the Cyclades, Aegean Sea, Greece: Part 1: geochronology. *Contrib Mineral Petrol* 160(5):719–742
- Bolhar R, Ring U, Kemp AIS, Whitehouse MJ, Weaver SD, Uysal IT, Turnbull R (2012) An integrated zircon geochronological and geochemical investigation into the Miocene plutonic evolution of the Cyclades, Aegean Sea, Greece: Part 2: geochemistry. *Contrib Mineral Petrol* 164(6):915–933
- Bolhar R, Ring U, Ireland TR (2017) Zircon in amphibolites from Naxos, Aegean Sea, Greece: origin, significance and tectonic setting. *J Metamorph Geol* 35(4):413–434
- Brichau S, Ring U, Ketcham RA, Carter A, Stockli D, Brunel M (2006) Constraining the long-term evolution of the slip rate for a major extensional fault system in the central Aegean, Greece, using thermochronology. *Earth Planet Sci Lett* 241(1):293–306
- Brichau S, Ring U, Carter A, Monié P, Bolhar R, Stockli D, Brunel M (2007) Extensional faulting on Tinos Island, Aegean Sea, Greece: how many detachments? *Tectonics* 26(4):TC4009. <https://doi.org/10.1029/2006TC001969>

- Buick IS, Holland TJB (1989) The PTt path associated with crustal extension, Naxos, Cyclades, Greece. *Geol Soc Lond Spec Publ* 43(1):365–369
- Cao S, Neubauer F, Bernroider M, Liu J (2013) The lateral boundary of a metamorphic core complex: the Moutsounas shear zone on Naxos, Cyclades, Greece. *J Struct Geol* 54:103–128
- Cao S, Neubauer F, Bernroider M, Genser J, Liu J, Friedl G (2017) Low-grade retrogression of a high-temperature metamorphic core complex: Naxos, Cyclades, Greece. *Geol Soc Am Bull* 129(1–2):93–117
- Chamberlin RT (1910) The Appalachian folds of central Pennsylvania. *J Geol* 18(3):228–251
- Dürr S, Altherr R, Keller J, Okrusch M, Seidel E (1978) The median Aegean crystalline belt: stratigraphy, structure, metamorphism, magmatism. *Alps Apennines Hellenides* 38:455–476
- Franz L, Okrusch M (1992) Aragonite-bearing blueschists on Arki island, Dodecanese, Greece. *Eur J Mineral* 4(3):527–537
- Gautier P, Brun JP, Jolivet L (1993) Structure and kinematics of Upper Cenozoic extensional detachment on Naxos and Paros (Cyclades Islands, Greece). *Tectonics* 12(5):1180–1194
- Gessner K, Gallardo LA, Markwitz V, Ring U, Thomson SN (2013) What caused the denudation of the Menderes Massif: review of crustal evolution, lithosphere structure, and dynamic topography in southwest Turkey. *Gondwana Res* 24:243–274
- Gibbs AD (1983) Balanced cross-section construction from seismic sections in areas of extensional tectonics. *J Struct Geol* 5(2):153–160
- Hansman R, Ring U (2018) Oligocene–Miocene trishear fault-propagation folding of the Jabal Hafit Anticline (UAE and Oman). *J Struct Geol* [in press (SG-2018-241)]
- Hossack JR (1979) The use of balanced cross-sections in the calculation of orogenic contraction: a review. *J Geol Soc* 136(6):705–711
- Jansen JBH (1973) Geological map of Greece, Island of Naxos (1:50,000). Institute for Geology and Mineral Resources, Athens
- Jansen JBH (1977a) The geology of Naxos, vol 19. Institute for Geology and Mineral Resources, Athens, pp 1–3
- Jansen JBH (1977b) Metamorphism on Naxos, Greece. Doctoral dissertation (Unpublished), Utrecht.
- Jansen JBH, Schuiling RD (1976) Metamorphism on Naxos; petrology and geothermal gradients. *Am J Sci* 276(10):1225–1253
- Jolivet L, Brun JP (2010) Cenozoic geodynamic evolution of the Aegean. *Int J Earth Sci* 99(1):109–138
- Keay S, Lister G, Buick I (2001) The timing of partial melting, Barrovian metamorphism and granite intrusion in the Naxos metamorphic core complex, Cyclades, Aegean Sea, Greece. *Tectonophysics* 342(3):275–312
- Kruckenber SC, Ferré EC, Teyssier C, Vanderhaeghe O, Whitney DL, Seaton NC, Skord JA (2010) Viscoplastic flow in migmatites deduced from fabric anisotropy: an example from the Naxos dome, Greece. *J Geophys Res Solid Earth* 115(B9):1978–2012
- Kuhlemann J, Frisch W, Dunkl I, Kázmér M, Schmiedl G (2004) Miocene siliciclastic deposits of Naxos Island: geodynamic and environmental implications for the evolution of the southern Aegean Sea (Greece). In: Bernet M, Spiegel C (eds) Detrital thermochronology—provenance analysis, exhumation, and landscape evolution of mountain belts, Special Paper 378. Geological Society of America, Boulder, pp 51–65
- Lévy F, Jaupart C (2011) Folding in regions of extension. *Geophys J Int* 185(3):1120–1134
- Linros H (2016) A 3-dimensional tectonic model of the Naxos metamorphic core complex, Greece. MSc-Thesis (Unpublished), Stockholms Universitet, Stockholm
- Lisker S (1993) The tectonosedimentary upper units of the Cyclades (Aegean Sea, Greece): A Paleogeographic and Tectonic Reconstruction. MSc-Thesis (Unpublished), Hebrew University, Jerusalem
- Lister GS, Forster M (1996) Inside the Aegean metamorphic core complexes. *Tech Publ Aust Crustal Res Centre* 45:110
- Martin L, Duchêne S, Delouie E, Vanderhaeghe O (2006) The isotopic composition of zircon and garnet: a record of the metamorphic history of Naxos, Greece. *Lithos* 87:174–192
- Maxelon M, Mancktelow N (2005) Three-dimensional geometry and tectonostratigraphy of the Pennine zone, Central Alps, Switzerland and Northern Italy. *Earth Sci Rev* 71(3–4):171–227
- Peillod A, Ring U, Glodny J, Skelton A (2017) An Eocene/Oligocene blueschist-/greenschist-facies PT loop from Naxos Island, (Cyclades, Greece): deformation-related re-equilibration vs thermal relaxation. *J Metamorph Geol* 35(7):805–830
- Rey PF, Teyssier C, Kruckenberg SC, Whitney DL (2011) Viscous collision in channel explains double domes in metamorphic core complexes. *Geology* 39(4):387–390. <https://doi.org/10.1130/G31587.1>
- Reiners PW, Brandon MT (2006) Using thermochronology to understand orogenic erosion. *Annu Rev Earth Planet Sci* 34:419–466
- Ring U, Gessner K, Güngör T, Passchier CW (1999) The Menderes Massif of western Turkey and the Cycladic Massif in the Aegean—do they really correlate? *J Geol Soc* 156(1):3–6
- Ring U, Layer PW, Reischmann T (2001) Miocene high-pressure metamorphism in the Cyclades and Crete, Aegean Sea, Greece: Evidence for large-magnitude displacement on the Cretan detachment. *Geology* 29(5):395–398
- Ring U, Will TM, Glodny J, Kumerics C, Gessner K, Thomson S, Okrusch M, Drüppel K (2007) Early exhumation of high-pressure rocks in extrusion wedges: Cycladic blueschist unit in the eastern Aegean, Greece, and Turkey. *Tectonics*. <https://doi.org/10.1029/2005TC001872>
- Ring U, Glodny J, Will TM, Thomson S (2010) The Hellenic subduction system: high-pressure metamorphism, exhumation, normal faulting, and large-scale extension. *Annu Rev Earth Planet Sci* 38:45–76
- Ring U, Gessner K, Thomson S (2017) Variations in fault-slip data and cooling history reveal corridor of heterogeneous backarc extension in the eastern Aegean Sea region. *Tectonophysics* 700:108–130
- Ring U, Glodny J, Peillod A, Skelton A (2018) The timing of high-temperature conditions and ductile shearing in the footwall of the Naxos extensional fault system, Aegean Sea, Greece. *Tectonophysics*. <https://doi.org/10.1016/j.tecto.2018.09.001>
- Robertson AHF, Clift PD, Degnan PJ, Jones G (1991) Palaeogeographic and palaeotectonic evolution of the Eastern Mediterranean Neotethys. *Palaeogeogr Palaeoclimatol Palaeoecol* 87(1–4):289–343
- Rösler HJ (1972) Das Neogen von Naxos und den benachbarten Inseln. *Zeitschrift der Deutschen Geologischen Gesellschaft* 123:523–525
- Sanchez-Gomez M, Avigad D, Heimann A (2002) Geochronology of clasts in allochthonous Miocene sedimentary sequences on Mykonos and Paros Islands: implications for back-arc extension in the Aegean Sea. *J Geol Soc London* 159:45–60
- Seward D, Vanderhaeghe O, Siebenaller L, Thomson S, Hibsich C, Zingg A, Duchêne S (2009) Cenozoic tectonic evolution of Naxos Island through a multi-faceted approach of fission-track analysis. *Geol Soc Lond Spec Publ* 321(1):179–196
- Thomson SN, Ring U, Bricchau S, Glodny J, Will TM (2009) Timing and nature of formation of the Ios metamorphic core complex, southern Cyclades, Greece. *Geol Soc Lond Spec Publ* 321(1):139–167
- Tomaschek F, Kennedy AK, Villa IM, Lagos M, Ballhaus C (2003) Zircons from Syros, Cyclades, Greece—recrystallization and mobilization of zircon during high-pressure metamorphism. *J Petrol* 44(11):1977–2002
- Urai JL, Schuiling RD, Jansen JBH (1990) Alpine deformation on Naxos (Greece). *Geol Soc Lond Spec Publ* 54(1):509–522

- Verrall P (1981) Structural interpretation, with application to north sea problems: course notes no. 3, 6–10th July 1981. Joint Association for Petroleum Exploration Courses (UK)
- Virgo S, von Hagke C, Urai JL (2018) Multiphase boudinage: a case study of amphibolites in marble in the Naxos migmatite core. *Solid Earth* 9(1):91–113
- Wijbrans JR, McDougall I (1988) Metamorphic evolution of the attic cycladic metamorphic belt on Naxos (Cyclades, Greece) utilizing $^{40}\text{Ar}/^{39}\text{Ar}$ age spectrum measurements. *J Metamorph Geol* 6(5):571–594
- Wijbrans JR, Schliestedt M, York D (1990) Single grain argon laser probe dating of phengites from the blueschist to greenschist transition on Sifnos (Cyclades, Greece). *Contrib Miner Petrol* 104(5):582–593
- Withjack MO, Peterson ET (1993) Prediction of normal-fault geometries—a sensitivity analysis. *AAPG Bull* 77(11):1860–1873
- Zanchi A, Salvi F, Zanchetta S, Sterlacchini S, Guerra G (2009a) 3D reconstruction of complex geological bodies: examples from the Alps. *Comput Geosci* 35(1):49–69
- Zanchi A, De Donatis M, Gibbs A, Mallet JL (2009b) Imaging geology in 3D. *Comput Geosci* 35(1):1–3